Korean J. Chem. Eng., **27**(1), 206-213 (2010)
DOI: 10.1007/s11814-009-0299-z

Investigation of cake deposition on various parts of the surface of microfiltration membrane due to fouling

Sayed Siavash Madaeni†, Masoud Rahimi, and Mahdiah Abolhasani

Membrane Research Center, Department of Chemical Engineering, Razi University, Kermanshah, Iran
(*Received 26 September 2008 • accepted 8 June 2009*)

Abstract−The accumulation of deposited layer on membrane surface in cross-flow microfiltration was investigated. This study provides a basis for elucidation of the membrane segments with superior tendency for cake deposition due to fouling. A commercially available GVWP membrane was fouled with a colored (blue indigo suspension in water) feed. The deposition pattern or fouling tendency was obtained using a digital camera, scanning electron microscope (SEM) and image analysis. The effects of feed concentration, transmembrane pressure and cross-flow velocity on cake deposition were investigated. In the early stages of the filtration trials, cake deposition was increased from the commencement portion (feed inlet) towards the furthermost part (concentrate outlet) of the membrane surface. However, at the completion of filtration, no pronounced difference was realized between cake deposition in the median and end parts of the membrane. Computational fluid dynamics (CFD) modeling of the membrane was carried out to predict the fouling behavior in various segments of the membrane at different operating conditions. The results of CFD modeling are in acceptable agreement with the experimental data. Accomplishment of the membrane sections with higher tendency for accumulation of foulants may provide a basis for manipulation of conditions to diminish the buildup of fouling deposition in the proposed segments. This results in lower cake deposition on vital parts to minimize the overall fouling.

Key words: Membrane, Microfiltration, CFD, Fouling, Cake Deposition

INTRODUCTION

Membrane fouling is the major deficiency encountering membrane processes. Numerous procedures have been put forth for characterization and minimization of fouling. Meng et al. [1] examined the effects of aeration intensity, concentration and sludge viscosity on the basis of hydrodynamics and rheology concepts. Zator et al. [2] characterized biofouling during microfiltration by scanning laser microscopy. Enevoldsen et al. [3] applied an electric field across the membrane to reduce the concentration polarization.

Geng et al. [4] investigated the mechanism of membrane fouling in pilot scale. Oh et al. [5] assessed fouling reduction of an integrated ozone and microfiltration process. Kim et al. [6] studied the dynamics of fouling of a microfilter by natural organic matter in serial filtration experiments. Metzger et al. [7] assessed the fouling layers and their effects on the fouling hydraulic resistance. Ang et al. [8] explored the influence of feed chemistry on the fouling of RO membranes by BSA. Meng et al. [9] figured out how sludge suspension impacts on membrane fouling. Chew et al. [10] studied the deposition of fouling layers on porous surfaces using the fluid Dynamic gauging (FDG) technique. Despite numerous researches in the field of fouling, there is a lack in fouling visualization.

Modeling in general and CFD in particular may be employed to understand and visualize fouling. Ahmad et al. [11] utilized CFD simulation to predict the concentration polarization profile as the basis for fouling. Chen et al. [12] inspected the complex nature of membrane fouling in the filtration of multi-component protein mixtures by examining the spatial distribution of protein foulants. Chen et al. [13] presented in situ monitoring techniques for concentration polarization and fouling. Chen et al. [14] reviewed the in situ observation of membranes.

In the present study, the deposition of blue indigo dye, as a colored foulant, on the surface of microfiltration membrane at various operating conditions of transmembrane pressure, cross-flow velocity and feed concentrations was experimentally studied using a lab scale cross-flow cell. The cake deposition on various segments of the membrane surface was determined. CFD modeling was employed to predict shear stress distribution on various parts of the membrane surface. This is a vital parameter influencing cake deposition.

MATERIALS AND METHODS

1. Apparatus

In all experiments, a cross-flow microfiltration system was used. Fig. 1 presents a schematic view of the experimental setup. The feed was pumped from the feed tank toward the cell. The inlet pressure and cross-flow velocity were controlled by the by-pass and outlet valves, respectively. The cell was made of Perspex. A schematic of internal space of cell is depicted in Fig. 2.

The membrane was placed on the top of a thin layer of porous rigid material as external support to prevent deformation of the membrane. The cross sectional area of the cell was 0.60 cm^2 and membrane surface area in contact with fluid was 23.65 cm^2.

2. Membrane

Polyvinylidenefluoride (PVDF) hydrophilic commercial membrane (GVWP) from Millipore was employed in this study. The average pore diameter of the membrane was 0.22 μm with 120 μm

†To whom correspondence should be addressed.
E-mail: smadaeni@yahoo.com

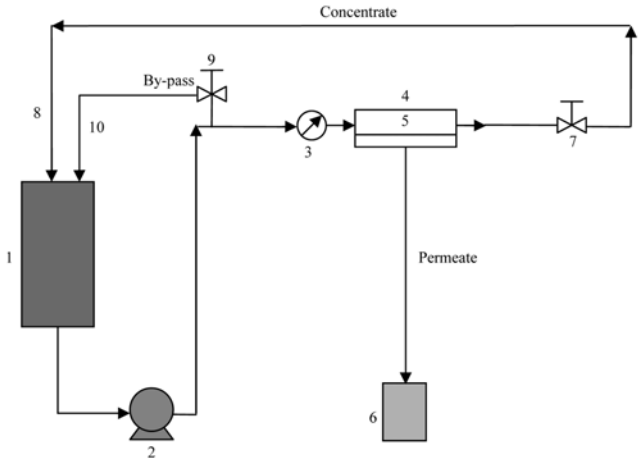

Fig. 1. Schematic of cross-flow microfiltration system.

1. Feed tank	6. Permeate
2. Pump	7. Outlet valve
3. Pressure gauge	8. Recycle stream
4. Cross-flow cell	9. By-pass valve
5. Membrane	10. By-pass stream

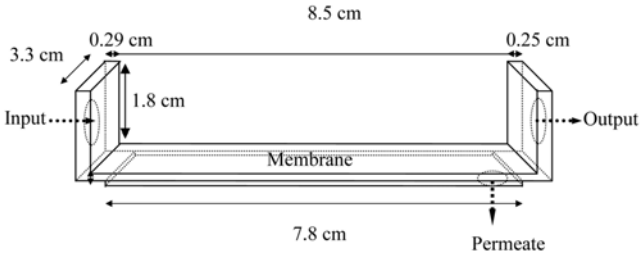

Fig. 2. The internal space of the cell with glass barrier.

Table 1. Different conditions for the conducted experiments

Experiments	Pressure (kPa)	Velocity (m/s)	Concentration (g/L)
a) Effect of pressure	100	1	0.05
	200	1	0.05
	300	1	0.05
b) Effect of velocity	100	0.5	0.05
	100	1	0.05
	100	1.3	0.05
c) Effect of concentration	100	1	0.025
	100	1	0.05
	100	1	0.1

thickness and 60% porosity.

3. Operating Conditions

A colored feed with different concentrations of 0.025, 0.05 and 0.1 g/L was passed through the membrane at transmembrane pressures of 100, 200 and 300 kPa and cross-flow velocities of 0.5, 1 and 1.3 m/s. The permeate flux was measured during 1, 5 and 20 minutes. A new membrane was employed for each trial. The different conditions for conducted experiment are listed in Table 1.

4. Image Analysis of Fouled Membrane

After each experiment, images of the fouled membranes were captured by digital camera. For image analysis Scion Image software was employed. Images are two dimensional arrays of pixels (picture elements) ranging in value from 0 to 255. Zero pixels are displayed as white and 255 pixels as black. The software generates a profile plot on the basis of rectangular selection on the image.

For further investigation, scanning electron microscope (SEM) micrographs from the beginning, median and end parts of the membranes were obtained. The membrane specimens were coated with platinum and viewed with SEM LEO1455VP at 10 kV.

5. CFD Modeling

An in-house 3D CFD code was employed to model the fluid flow hydrodynamics inside the membrane cell. To explain the dye deposition on the membrane surface, the predicted distribution of shear stress on the membrane surface was analyzed. High shear stress decreases the possibility of adhesion between particles and membrane surface. This results in lower fouling.

The CFD modeling involves the numerical solution of the conservation equations in the laminar and turbulent fluid flow regimes. In general, it is most attractive to characterize the turbulent flow by the mean values of flow properties and the statistical properties of their fluctuations. Introducing the time-averaged properties for the flow to the time dependent Navier-Stokes equations, led to time-averaged Navier-Stokes equations as follows [15]:

Continuity equation:

$$\frac{\partial}{\partial t}(\rho)+\nabla\cdot(\rho \mathrm{V})=0 \tag{1}$$

Where t is time, ρ is the density and V is the velocity vector.

Momentum equation:

$$\frac{\partial}{\partial t}(\rho \mathrm{V})+\nabla\cdot(\rho \mathrm{V}\mathrm{V})=\nabla\cdot((\mu+\mu_t)\nabla \mathrm{V})+\mathrm{F} \tag{2}$$

Where V is velocity vector, ρ is density and F is the momentum source term. In addition, μ_t is the turbulent viscosity which should be obtained from a turbulence model. In this study, the RNG version of k-ε model was employed as the turbulence model with its default parametric values [16].

In the model, the cell was meshed into 92817 control volumes. No-slip boundary condition was assumed for all surrounding walls. The SIMPLE pressure-velocity coupling algorithm, the standard pressure, the second order upwind discretization scheme for momentum, turbulent kinetic energy and dissipation energy were used in

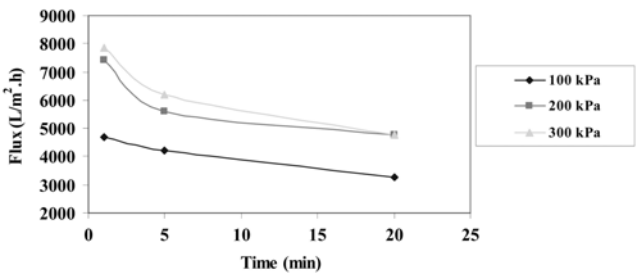

Fig. 3. Effect of transmembrane pressure on flux (cross-flow velocity 1 m/s, feed concentration 0.05 g/L).

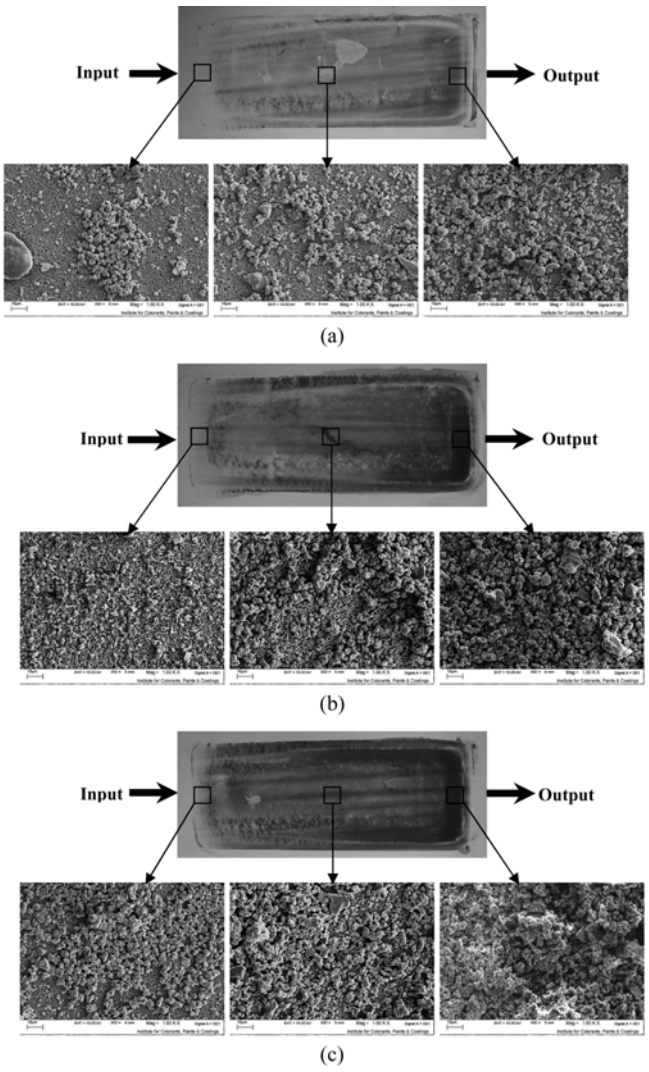

Fig. 4. Digital images and SEM micrographs of various parts of the GVWP membrane surface fouled by blue indigo dye at different transmembrane pressures after 1 min filtration (cross-flow velocity 1 m/s, feed concentration 0.05 g/L) (a) 100 kPa (b) 200 kPa (c) 300 kPa.

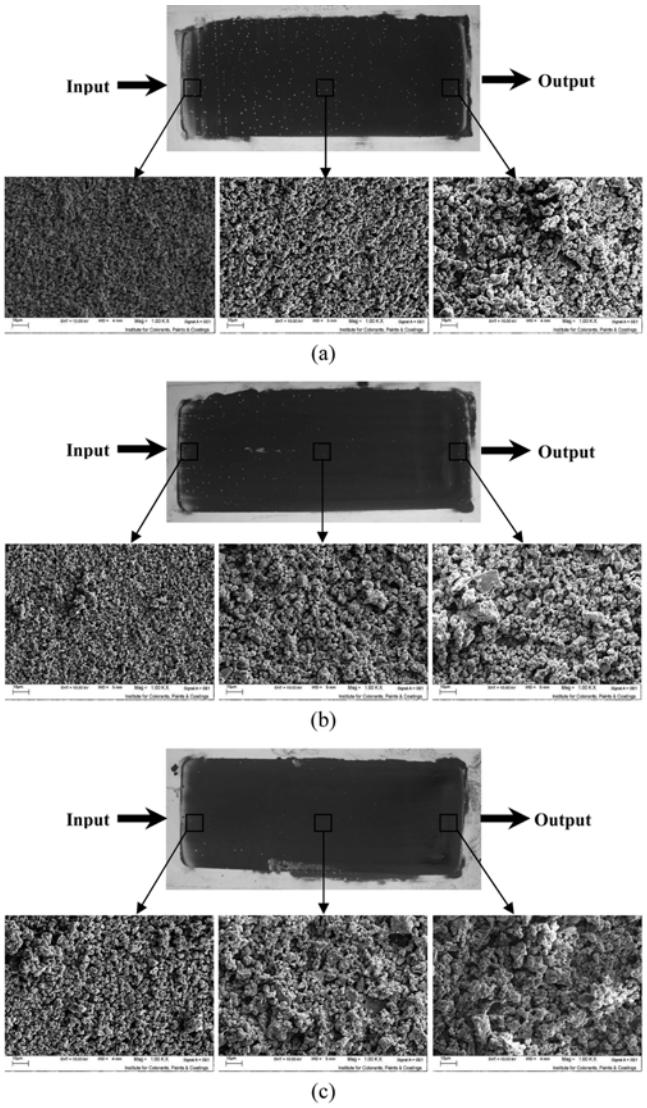

Fig. 5. Digital images and SEM micrographs of various parts of the GVWP membrane surface fouled by blue indigo dye at different transmembrane pressures after 20 min filtration (cross-flow velocity 1 m/s, feed concentration 0.05 g/L) (a) 100 kPa (b) 200 kPa (c) 300 kPa.

the model. In addition, a convergence criterion of 10^{-4} was chosen for all calculated parameters [17].

RESULTS AND DISCUSSION

1. The Effect of Transmembrane Pressure on Cake Deposition

Fig. 3 illustrates the flux as a function of transmembrane pressure. Particles gradually move towards the membrane and deposit on the surface. This results in flux decline. The deposition at the beginning, median and furthermost segments of the membranes (compared to feed inlet) is clearly visible in SEM micrographs. Figs. 4 and 5 represent the images after one and 20 minutes filtration, respectively. The images illustrate the differences in diverse sections of the fouled membrane at various transmembrane pressures. The minimum and maximum depositions appeared at 100 and 300 kPa, respectively. For all transmembrane pressures, accumulation of blue indigo particles extended from the beginning part (feed inlet) towards the end part (concentrate outlet) of the membranes. Fig. 6 indicates that there is no pronounced difference between the deposition on the median and end segments after 20 minutes.

In summary, the thickness of the fouling layer grows from feed inlet towards the concentrate outlet of the membrane. The highest transmembrane pressure exhibits maximum accumulation compared to the lower pressures at all parts of the membrane surface.

To verify the results from SEM micrographs and exhibit the accumulation of indigo dye on the membrane surface, the Scion Image software was employed. The obtained profiles are illustrated in Fig. 7. This figure is density profile plot based on the rectangular selection around the grey scale digital images. Plot profile option of Scion Image software generates this kind of plot. The software produces a "column average plot." The width of the plot is equal to the membrane length. Each point in the plot represents the average grey value of the pixels in the corresponding column in the membrane. The

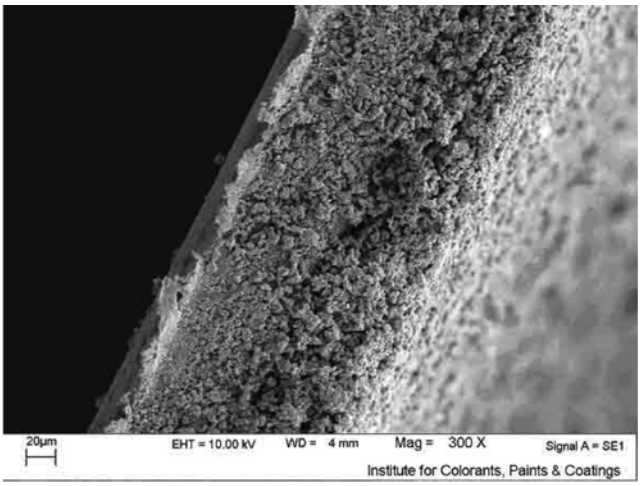

(a)

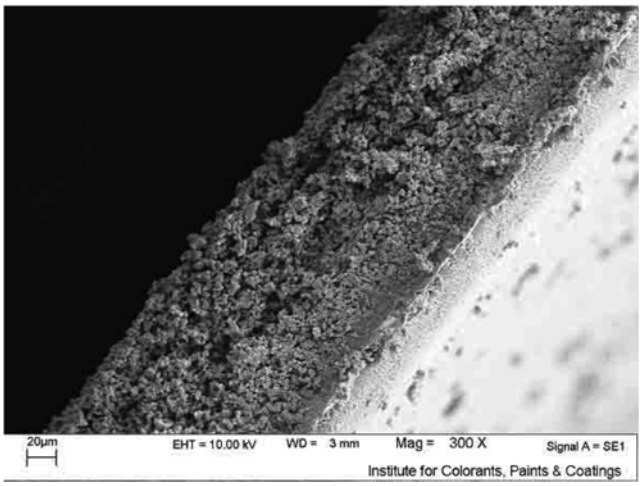

(b)

Fig. 6. Cross sectional SEM micrographs of middle and end parts of the membrane after 20 minutes filtration (Transmembrane pressure 300 kPa, velocity 1 m/s, feed concentration 0.05 g/L) (a) middle part (b) end part.

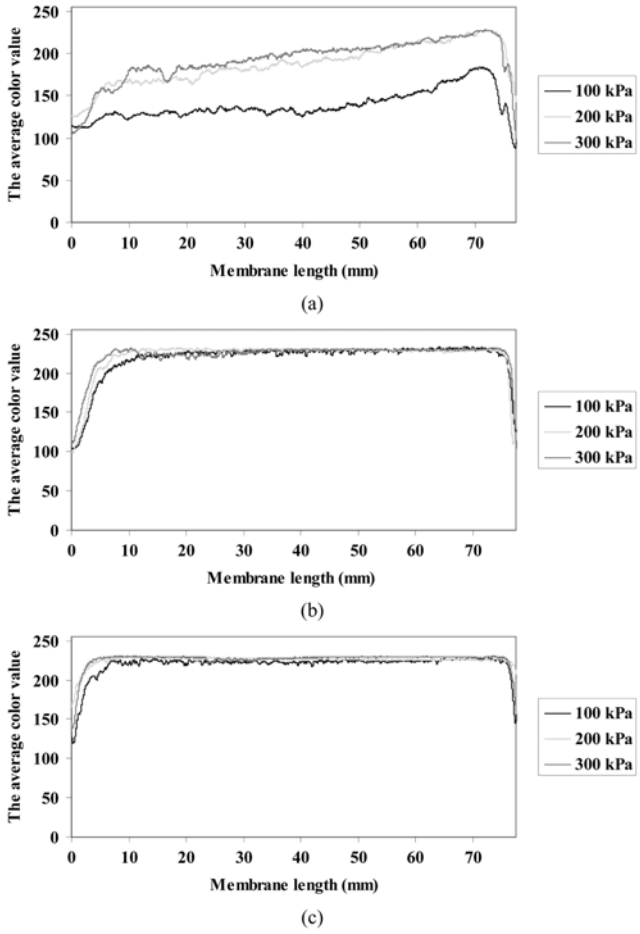

Fig. 7. Comparison of the average color values on the membrane surface at different transmembrane pressures (cross-flow velocity 1 m/s, feed concentration 0.05 g/L) after (a) 1 minute (b) 5 minutes (c) 20 minutes filtration.

X-axis is the pixel location (length of the membrane) and Y-axis is the indicator of average color value of pixels constituting the width of the membrane. The uncalibrated pixel grey values range from 0 for white color to 255 for black.

At 100 and 300 kPa the color values on the membrane surface are the lowest and highest, respectively. For all cases, at the commencement segments, the color value is minimum, indicating the lowest accumulation of blue indigo particles.

As the filtration duration exceeds from 1 to 20 minutes, the color value on the membrane surface is increased. However, the rate of color increment in the beginning portion is much higher compared to the color expansion at the end part of the membrane surface.

The accumulations of deposit on the membrane surface at the commencement parts are minimal. This may be explained on the basis of the higher capability of the flowing feed for removal of deposits at the entering part. The fluid feed is able to wash the accumulated deposit on the membrane surface and prevents the sedimentation of particles. The effectiveness of this process is higher at the entrance of the membrane cell. Therefore, the generated layer at the starting point on the membrane surface is thinner and its resistance is accordingly lower.

Fig. 8 represents the CFD modeling of the shear stress distribution on the membrane surface. The segments with lower shear stress provide the conditions for higher deposition of foulants on the membrane surface. This figure clearly indicates these locations. The shear stress decreases from the beginning segments of the membrane towards the furthermost parts, i.e., the deposition of foulants should decrease from start to the end. This is in agreement with the observed cake deposition in Fig. 4. Fig. 8 indicates that there is no difference between shear stress distributions for various transmembrane pressures. This emphasizes the limited capability of CFD modeling for prediction of all conditions in membrane processes.

2. The Effect of Cross-flow Velocity on Cake Deposition

The effects of cross-flow velocity were investigated at 0.5, 1 and 1.3 m/s. Fig. 9 shows that higher cross-flow velocity results in higher flux. SEM micrographs of cake deposition from the beginning, median and end parts of the membrane surface after 1 and 20 minutes filtration are depicted in Figs. 10 and 11. The differences between various sections of the fouled membranes can be viewed by the naked eye. The maximum deposition was realized with the lowest cross-

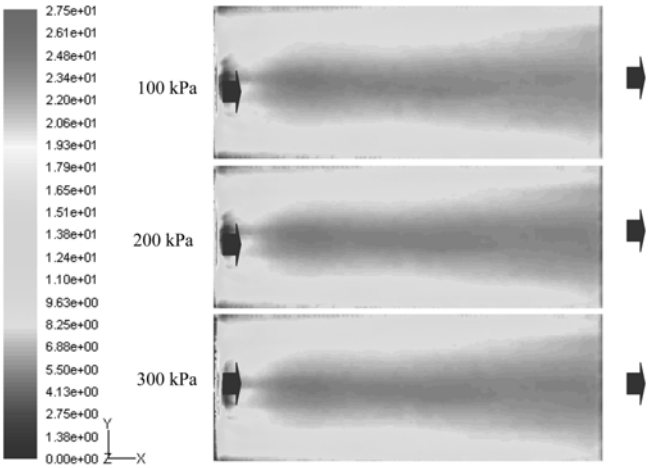

Fig. 8. Distribution of wall shear stress (Pa) on the membrane surface at various transmembrane pressures (Cross-flow velocity 1 m/s, concentration 0.05 g/L).

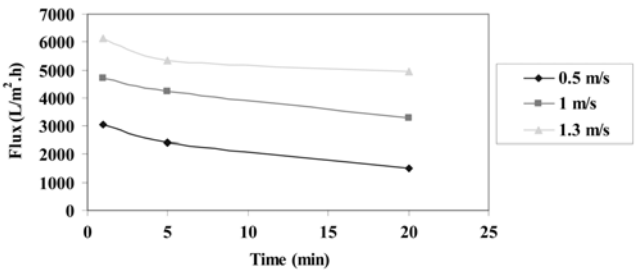

Fig. 9. Effect of cross-flow velocity on permeate flux (transmembrane pressure 100 kPa, feed concentration 0.05 g/L).

flow velocity of 0.5 m/s and the minimum fouling appeared at 1.3 m/s. For all velocities, fouling or accumulation of blue indigo particles grows from the beginning towards the end segments. For longer filtration times, the accumulated particles in the median and end sections are almost similar.

Fig. 12 illustrates the profiles of fouled membrane images. At cross-flow velocity of 0.5 m/s the color value on the membrane surface is highest, indicating the most accumulated blue indigo particles on the membrane surface. At 1.3 m/s the color values are lowest. At the early stages of all cases, the color value is minimal.

To explain the dye deposition on the membrane surface, the distributions of wall shear stress on the membrane surface at various cross-flow velocities were obtained. The results presented in Fig. 13 were analyzed. The high shear stress decreases the possibility of cohesion between the particles and surface. This results in fouling decline.

The CFD pattern indicates that membrane fouling at the central region is more than the lateral side. Moreover, the counters show that fouling is low at the cell entrance compared to the end of the cell. The CFD modeling predicts higher shear stress for higher linear velocity on the membrane surface. This is in agreement with the experimental results indicated in Fig. 10. The shear stress decline (i.e., more deposition of foulants) from start to the end of membrane length is observable for highest cross-flow velocity. For lower

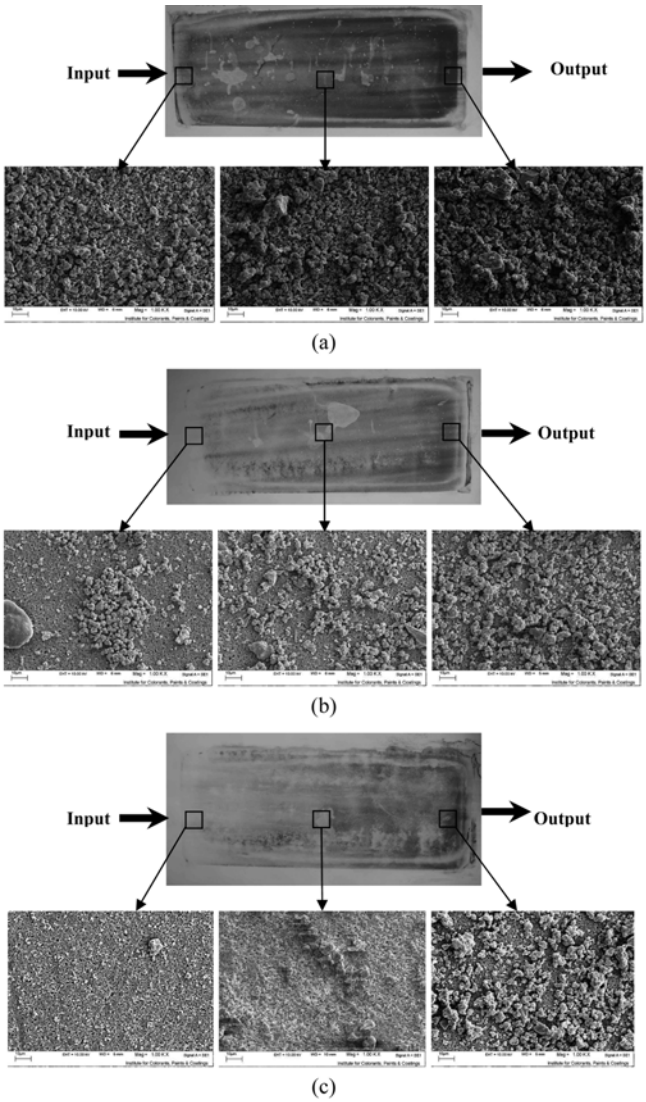

Fig. 10. Digital images and SEM micrographs of various parts of the GVWP membrane surface fouled by blue indigo dye at different cross-flow velocities after 1 min filtration (transmembrane pressure 100 kPa, feed concentration 0.05 g/L) (a) 0.5 m/s (b) 1 m/s (c) 1.3 m/s.

velocities this is less predictable.

3. The Effect of Feed Concentration on Cake Deposition

The effect of feed concentration on flux was investigated at 0.025, 0.05 and 0.1 g/L. Increasing the feed concentration leads to flux decline. SEM micrographs from the beginning, median and end parts of the membranes are depicted in Figs. 14 and 15.

Cake deposition depends on the feed concentration being higher for higher concentrations. The accumulation of blue indigo particles grows from the beginning part towards the end section of membranes. The deposition is low at the early stages. At the beginning part, flowing feed may wash and remove the accumulated particles on the membrane surface. Therefore, the generated layer at the commencement segment of the membrane surface is thinner with lower resistance. At the middle and end parts, the maximum concentration provides larger cake deposition. Feed concentration influences the particle adsorption on the membrane surface.

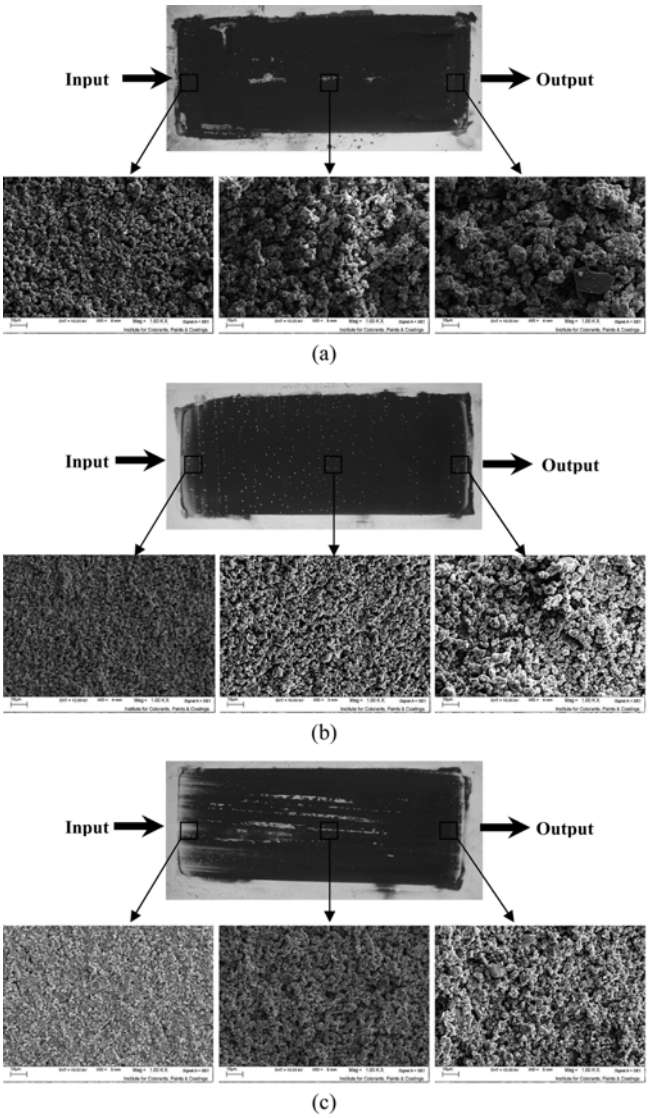

Fig. 11. Digital images and SEM micrographs of various parts of the GVWP membrane surface fouled by blue indigo dye at different cross-flow velocities after 20 min filtration (transmembrane pressure 100 kPa, feed concentration 0.05 g/L) (a) 0.5 m/s (b) 1 m/s (c) 1.3 m/s.

Fig. 16 illustrates the profiles of a fouled membrane. For lower feed concentration, the color values on the membrane surface are minimal. This represents the least accumulation of blue indigo particles on the membrane surface. For all cases at the beginning part, the color value is minimal, reflecting the effect of maximum shear stress.

The previously presented CFD patterns in Figs. 8 and 13 illustrate the variation of shear stress for a specific concentration (0.05 g/L) at different operating conditions of transmembrane pressures and cross-flow velocities. This explains the non-uniform distribution of the cake deposition on the membrane surface. However, CFD modeling is not able to differentiate between various feed concentrations.

4. Non-uniformity of Cake Formation, Explanations and Consequences

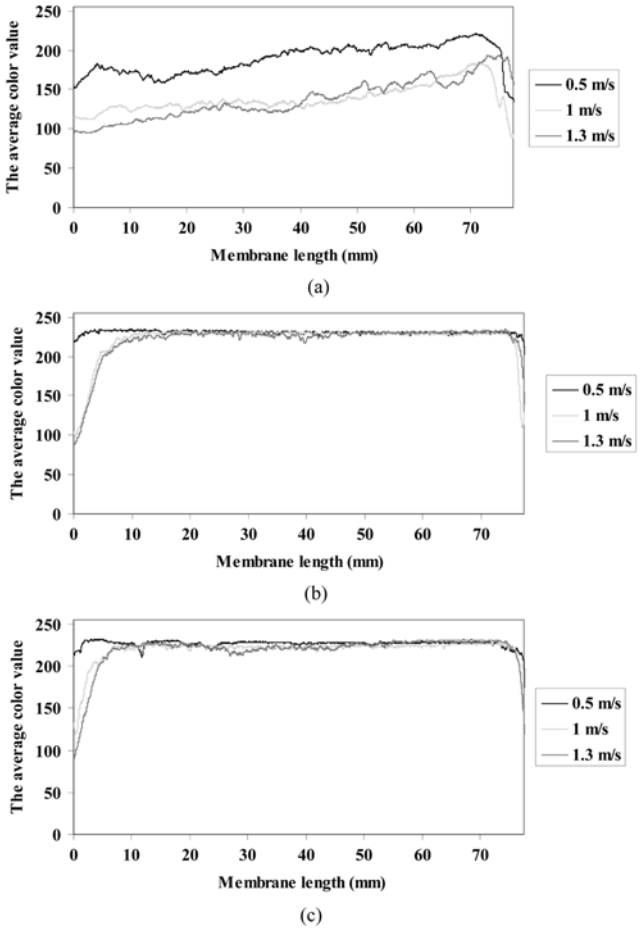

Fig. 12. Comparison of the average color values on the membrane surface at different cross-flow velocities (transmembrane pressures 100 kPa, feed concentration 0.05 g/L) after (a) 1 minute (b) 5 minutes (c) 20 minutes filtration.

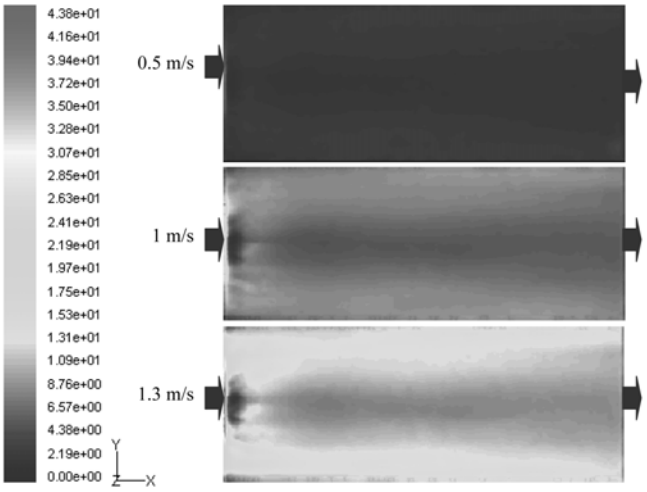

Fig. 13. Distribution of wall shear stress (Pa) on the membrane surface at various cross-flow velocities (transmembrane pressures 100 kPa, concentration 0.05 g/L).

As a summary of previously presented facts and figures, we may emphasize that a non-uniform cake layer is deposited on the mem-

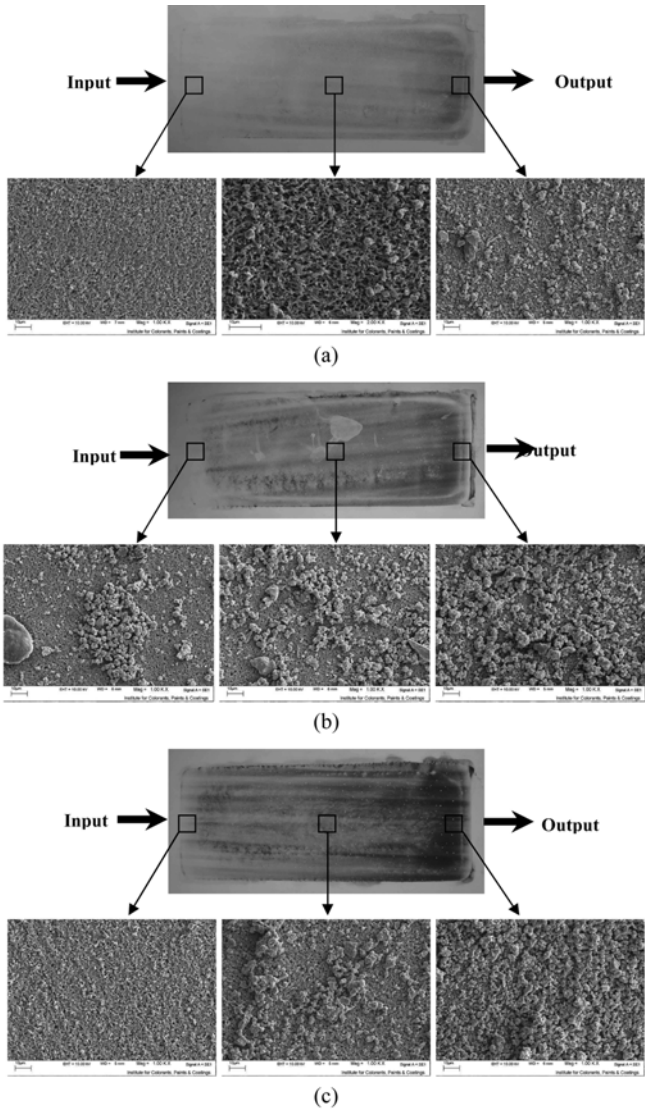

Fig. 14. Digital images and SEM micrographs of various parts of the GVWP membrane surface fouled by blue indigo dye at different feed concentrations after 1 min filtration (transmembrane pressure 100 kPa, cross-flow velocity 1 m/s) (a) 0.025 g/L (b) 0.05 g/L (c) 0.1 g/L.

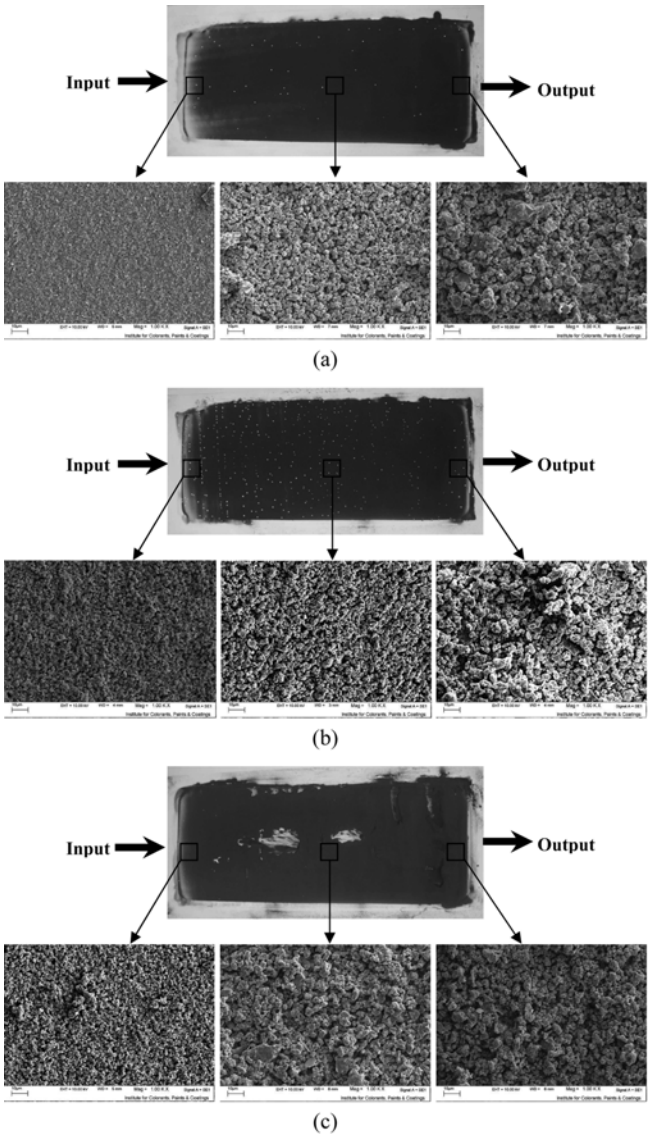

Fig. 15. Digital images and SEM micrographs of various parts of the GVWP membrane surface fouled by blue indigo dye at different feed concentrations after 20 min filtration (transmembrane pressure 100 kPa, cross-flow velocity 1 m/s) (a) 0.025 g/L (b) 0.05 g/L (c) 0.1 g/L.

brane surface. Although the creation of fouling layer depends on the overall operating conditions, including transmembrane pressure, cross-flow velocity and feed concentration, the non-uniformity of the cake layer was observed for all conditions.

In general, creation of a fouling layer is slim at the beginning part and is thick and wide in the end sections of the membrane surface regardless the operation conditions. This is due to the discrepancy of operating conditions on various parts of the membrane surface. Non-uniform operating conditions on the membrane surface result in variable and diverse cake formation through the cell. The effect of induced shear stress on cake formation is well-known. The overall shear stress may be considered constant for practical purposes. However, this is not true for all single points of the membrane surface. CFD simulation confirms the non-uniformity of shear stress on various parts of the membrane surface. This results in higher cake deposition in the spots with lower shear stress.

Cross-flow velocity affects the cake formation due to turbulence conditions at higher velocities. However, the distribution of cross-flow velocity on various locations of the membrane surface is not consistent. The evidence is observable by CFD modeling in Fig. 17. The cross-flow velocity is higher at the feed entrance. This condition is more favorable for removing particles from the membrane surface with less deposition of fouling layer on the membrane surface.

This study represents a rationale for better understanding of cake deposition on various parts of the membrane surface. Realization of the points or parts with higher accumulation of foulants may lead to manipulation of operating conditions to diminish the buildup of fouling layers in those specific parts. This results in lower cake deposition on vital places to minimize the overall fouling.

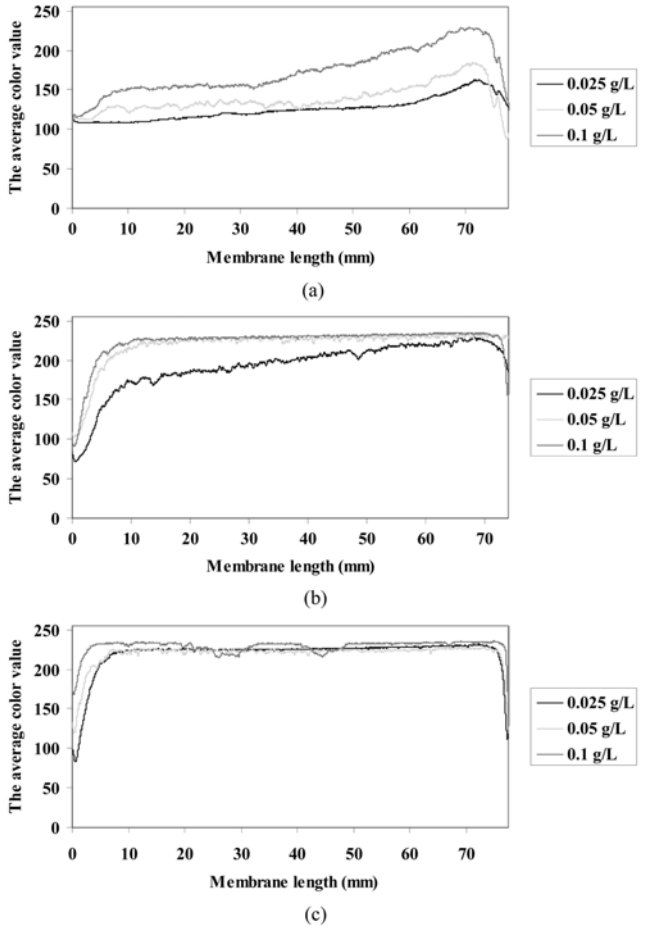

Fig. 16. Comparison of average color values on the membrane surface at various feed concentrations (transmembrane pressure 100 kPa, cross-flow velocities 1 m/s) after (a) 1 minute (b) 5 minutes (c) 20 minutes filtration.

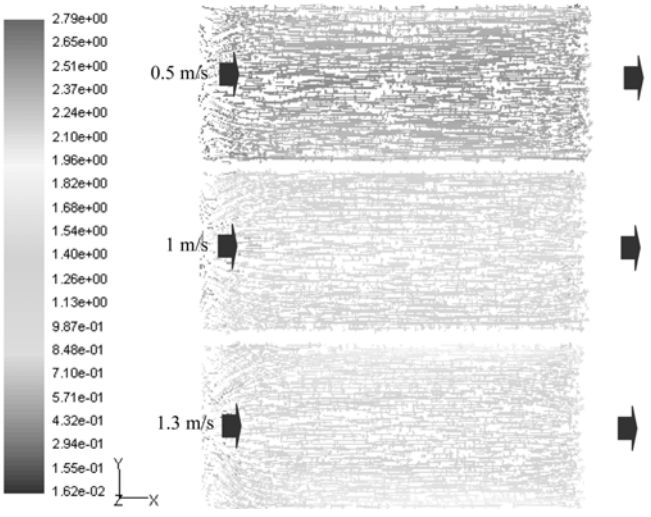

Fig. 17. Distribution of velocity (m/s) on the membrane surface at various overall cross-flow velocities (transmembrane pressures 100 kPa, concentration 0.05 g/L).

CONCLUSION

The aggregation and accumulation of particles on the membrane surface leads to membrane fouling. These layers create additional resistance, resulting in flux decline. In cross-flow microfiltration, as the flowing feed enters the cell it can sweep away the particles and remove them from the entering point of the cell and accumulate them at the furthermost parts of the membrane surface. The cake layer formation is a function of operating conditions such as transmembrane pressure, cross-flow velocity and feed concentration. However, the creation of a fouling layer is slim at the beginning part and is thick and wide in the end parts of the membrane surface, regardless of the operation conditions. This is due to the discrepancy of operating conditions on various parts of the membrane surface. Non-uniform operating conditions on the membrane surface result in variable and diverse cake formation throughout the cell.

REFERENCES

1. F. Meng, B. Shi, F. Yang and H. Zhang, *J. Membrane Sci*., **302**, 87 (2007).
2. M. Zator, M. Ferrando, F. L´opez and C. Guell, *J. Membrane Sci*., **301**, 57 (2007).
3. A. D. Enevoldsen, E. B. Hansen and G. Jonsson, *J. Membrane Sci*., **299**, 28 (2007).
4. Z. Geng, E. R. Hall and P. R. Berube, *J. Membrane Sci*., **296**, 93 (2007).
5. B. S. Oh, H. Y. Jang, Y. J. Jung and J. W. Kang, *J. Membrane Sci*., **306**, 244 (2007).
6. J. Kim, W. Shi, Y. Yuan and M. M. Benjamin, *J. Membrane Sci*., **294**, 115 (2007).
7. U. Metzger, P. Le-Clech, R. M. Stuetz, F. H. Frimmel and V. Chen, *J. Membrane Sci*., **301**, 180 (2007).
8. W. S. Ang and M. Elimelech, *J. Membrane Sci*., **296**, 83 (2007).
9. F. Meng and Y. Yang, *J. Membrane Sci*., **305**, 48 (2007).
10. Y. M. J. Chew, W. R. Paterson and D. I. Wilson, *J. Membrane Sci*., **296**, 29 (2007).
11. A. L. Ahmad, K. K. Lau, M. Z. Abu Bakar and S. R. Abd. Shukor, *Comput. Chem. Eng*., **29**, 2087 (2005).
12. V. Chen, R. Chan, H. Li and M. P. Bucknall, *J. Membrane Sci*., **287**, 79 (2007).
13. J. C. Chen, Q. Li and M. Elimelech, *Adv. Colloid Interfac*., **107**, 83 (2004).
14. V. Chen, H. Li and A. G. Fane, *J. Membrane Sci*., **241**, 23 (2004).
15. H. K. Versteeg and W. Malalasekera, An Introduction to Computational Fluid Dynamics, The Finite Volume Method, Longman Limited, England (1995).
16. V. Yakhot and S. A. Orszag, *J. Sci. Comput*, **1**, 1 (1986).
17. M. Abolhasani, M. Rahimi and S. S. Madaeni, *CFD and experimental study on microfiltration fouling in different operating pressure*, The first National Conference on CFD Application in Chemical Engineering, 14-15 May 2008, Kermanshah, Iran.